Precision Measurement of the g Factor of the Free Electron*

D. T. WILKINSON AND H. R. CRANE
Harrison M. Randall Laboratory of Physics, University of Michigan, Ann Arbor, Michigan
(Received 21 December 1962)

The measurement reported is essentially a refinement of an earlier measurement in which the g factor was found to ± 2.4 parts in 10^6. The method is as follows: 100-keV electrons in 0.2-μsec bunches move parallel to a magnetic field and strike a gold foil. The part of an electron bunch which is scattered at right angles, and which, consequently, is partially polarized, is trapped in the magnetic field and held for a measured length of time (up to 1.9 msec). The bunch is then released from the trap and allowed to strike a second gold foil. The cycle is repeated 500 times per sec. The part of the bunch scattered at right angles by the second foil strikes a thin-window Geiger counter. The fraction of the bunch scattered into the counter depends upon its final direction of polarization. A plot of the intensity vs trapping time is a cosine curve whose frequency is the difference between the orbital frequency and the spin precession frequency. This is related to the g factor as follows: $\omega_D mc/Be=a$, where g is $2(1+a)$, ω_D is 2π times the difference frequency, B is the magnetic induction, and m, c, and e have the usual meaning. Thus the "anomaly," a, is measured directly. The present experiment is an advance over the earlier one in four main respects: (a) Separation of the polarization effect from the background. Alternate groups of 64 electron bunches were held in the trap for times t and $t+\frac{1}{2}T_D$, where T_D is the period of alternation of intensity or "difference period." Counts from the alternate bunches were accumulated in separate scalers, and the ratio was used as the measure of polarization. This eliminated virtually all instrumental asymmetries associated with counting. (b) Electrostatic effects. A new vacuum chamber in which all material was eliminated from inside the electron orbits and removed to a greater distance from the orbits on all sides greatly reduced the effects of stray electric fields due to surface charges. (c) Magnetic field. A new solenoid of increased dimensions, and new proton-resonance field measuring apparatus were used, to obtain a significant improvement in the mapping of the magnetic field in the trap. (B appears in the formula for a, and in order to have a trap, B must be slightly nonuniform; hence the necessity of mapping B in the trap.) (d) The beginning of the measured trapping interval was moved out to about 300 μsec after injection and a time difference method was used. This eliminated all errors associated with initial structure (bunching) of the electron cloud, and eliminated errors in the knowledge of the time of injection and capture. The final result is $a=0.001\,159\,622\pm0.000\,000\,027$. In terms of a series in the fine structure constant, the experiment gives $a=\alpha/2\pi-(0.327\pm0.005)\alpha^2/\pi^2$ and theory gives $a=\alpha/2\pi-0.328\alpha^2/\pi^2$.

I. INTRODUCTION

THE measurement reported here is the third and final in a series of three measurements on the g factor of the free electron, which have been carried on in this laboratory over the past decade. All of the experiments employed a Mott double scattering arrangement, with a magnetic field interposed between the polarizing and analyzing scatterers. In the first experiment[1] the magnetic field was parallel to the electron paths. The g factor was determined by measuring the rotation of the plane of polarization in the magnetic field, and the other parameters. The result ($g=2.00\pm0.01$) was not sufficiently precise to be useful theoretically. The interest in the experiment lay in the fact that it brought about the resolution of some questions as to the measurability, in principle, of the g factor of the electron in the free state, and opened the way to experiments of greater precision.

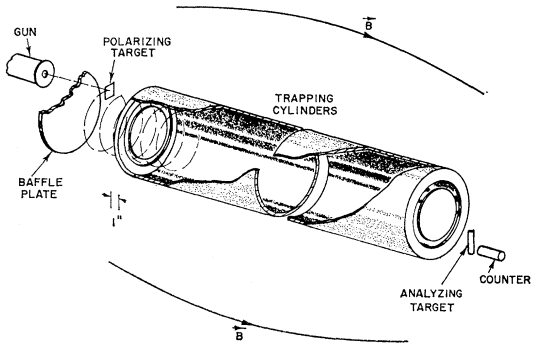

FIG. 1. Schematic drawing of the internal components in the trapping region.

In the second experiment,[2] two basic improvements in method were introduced: (a) The electrons were trapped in a magnetic "bottle" so that the number of revolutions of the polarization plane could be very large, and (b) the difference between the spin precession frequency and the cyclotron frequency, rather than the spin precession frequency itself, was measured. The result of the second experiment was $g=2(1+0.0011609\pm0.0000024)$. In spite of the very great improvement in accuracy, this result fell just short of what was to be hoped for, in that the uncertainty was just about equal to the value of the α^2 term in the theoretical result. This was made evident by writing the result of the second experiment and the theoretical result as series in α: $a=\alpha/2\pi-0.328\alpha^2/\pi^2$ (theory); $a=\alpha/2\pi-(0.1\pm0.4)\alpha^2/\pi^2$ (exp), where $g=2(1+a)$. The fact of being so near to a fully significant result caused the present authors to undertake a third, and entirely new,

* This work is supported by the Atomic Energy Commission.
[1] W. H. Louisell, R. W. Pidd, and H. R. Crane, Phys. Rev. **94**, 7 (1954).
[2] A. A. Schupp, R. W. Pidd, and H. R. Crane, Phys. Rev. **121**, 1 (1961).

measurement. The outcome exceeded our minimum goal of $\pm 10\%$ of the α^2 term, and gave it to within less than 2%. Consequently, we have dared to label the third experiment the "final" one in the series.

II. GENERAL DESCRIPTION OF THE METHOD

Scattering and Trapping

Attention is called to Fig. 1. A bunch of electrons from the gun, moving parallel to the axis of the chamber, is scattered by a thin gold target. A slit system (not shown in the figure) allows only those electrons which are scattered to the right, through an angle of about 89°, to leave the vicinity of the foil. There is present a fixed magnetic field whose axis of symmetry coincides with the axis of the chamber, and which is slightly shaped so as to form a "bottle" for the electrons. The magnetic center of the bottle is at the gap between the two cylinders seen in Fig. 1. The electrons which emerge from the slits, after being scattered, begin a helical motion in the bottle with a pitch of about 1°. When the bunch starts its journey, there is a retarding potential difference across the gap between the two cylinders. As the bunch progresses from left to right across the gap, the pitch decreases, because of the potential difference. The bunch continues some distance to the right and is reflected from the right-hand end of the magnetic bottle. Before the bunch recrosses the gap, the potential difference is reduced to zero. Thus the pitch remains reduced and the bunch cannot return as far to the left as the position of the slits. After holding the electrons in the bottle for an arbitrary length of time, an electric potential difference is applied to the gap which accelerates electrons to the right. Then all those electrons which happen to be in the left-hand cylinder at the time are able to escape out of the right-hand end of the bottle. (It should be mentioned that after the electrons have been in the trap for about 50 μsec or more they are no longer bunched, so about half of them are ejected regardless of the timing.) The ejected electrons move out of the trap in a helix, and strike a second gold foil—the analyzing target. The ones which are scattered at about 90°, into a direction parallel to the axis of the chamber, strike a thin-window Geiger counter. The sequence is repeated 500 times per sec.

Polarization Direction and Detection of Polarization

In the first scattering process, partial polarization of the electron beam occurs, the direction of polarization being along the radius of the helix. During the time the electrons are in the trap, the direction of polarization rotates around an axis parallel to the magnetic field. If the time between first and second scattering is such that an integral number of half-revolutions is made, the electrons will strike the second scatterer with their polarization direction again lined up with the radius of the helix. This is the condition for maximum right-left asymmetry in intensity of scattering from the second foil. Only one counter is used in the geometrical position shown in Fig. 1. The fraction of the electron bunch scattered into this counter is a function of the angle between the direction of polarization and the radius; more specifically, if θ is the angle, the fraction scattered into the counter is $A+\delta\cos\theta$ where in a typical case δ is about 5% of A.

Quantitative Relations

The orbital, or cyclotron angular velocity is $\omega_c=\omega_0/\gamma$, where ω_0 is the "zero-energy" cyclotron angular velocity or eB/mc; γ is $(1-v^2/c^2)^{-1/2}$; B is the magnetic induction; e and m are the charge and mass of the electron, respectively; and v and c are the velocity of the electron and the velocity of light, respectively. The spin precession angular velocity, for electrons moving perpendicular to the magnetic field is[3]

$$\omega_s=\omega_0(1/\gamma+a), \tag{1}$$

where a is the "g-factor anomaly" in $g=2(1+a)$. Since the analyzing assembly has a fixed azimuthal position, the final direction of polarization changes with time according to the beat, or difference between ω_c and ω_s. The two equations above yield the simple relation: $\omega_D=\omega_0 a$, and the observable quantity, ω_D, is a direct measure of the g-factor anomaly.

For measurements of such precision as we are attempting, certain refinements must be introduced into Eq. (1). These take into account: (1) the inhomogeneity of the magnetic field in the trapping region, (2) the finite pitch of the trapped beam, (3) stray radial electric fields, and (4) a possible electric dipole moment (EDM) for the electron. Ford[4] has obtained an expression for ω_s which includes these effects. Using Ford's result, and denoting the time average by a bar[5] or by $\langle\ \rangle_{\rm av}$, we get the following expression for the difference frequency expected in this experiment:

$$\frac{\omega_D}{\omega_0}=a-\frac{a\gamma}{\gamma+1}\frac{\langle v_z^2\rangle_{\rm av}}{c^2}-\frac{1}{\beta\gamma^2}\frac{\bar{E}_r}{\bar{B}_z}+\frac{f^2\beta^2}{8a}, \tag{2}$$

where β is v/c, v_z is the axial component of velocity in the trap, E_r is the radial electric field, B_z is the axial component of the magnetic field, and $f/2$ is the EDM in Bohr magnetons. The first correction term following a is due to the finite pitch of the trapped beam. It should be noted that only a quadratic term appears, since terms which are linear in v_z go to zero when averaged over a time large compared to the period of axial oscillation. The second correction term is due to

---

[3] H. Mendlowitz and K. M. Case, Phys. Rev. **97**, 33 (1955).
[4] G. W. Ford (private communication).
[5] Although the electric and magnetic fields do not change with time, electrons move, so the time average of the field experienced by the trapped electrons must be estimated and used.

stray radial electric fields, whose effect is mainly to shift the cyclotron frequency. The third correction term gives the effect of a possible electric dipole moment for the electron. In Sec. V, Eq. (2) is applied to the data of the experiment to find the value of a.

Method of Observing and Measuring the "Difference Frequency"

A single counter serves to measure the intensity asymmetry in the scattering from the analyzing target. The counts from 64 bunches of electrons, which have been trapped for a time t, are fed into one scaler. Then the trapping time is shifted to $t+\frac{1}{2}T_D$ (where T_D is the period of rotation of the polarization direction at the analyzing target), and the counts from the next 64 bunches are fed into a second scaler. The apparatus automatically alternates between these two settings, until sufficient data have accumulated in the two scalers. Since a shift in time of $\frac{1}{2}T_D$ has the effect of inverting the polarization, it is equivalent to moving the counter to the opposite side of the analyzing target. The ratio of the counting rates in the two scalers (asymmetry) is measured and plotted as a function of trapping time. This gives a cosine curve, which yields ω_D. The advantage gained by using a single counter in this way instead of using the more conventional arrangement of two counters on opposite sides of the target is that all problems associated with differences in sensitivity, solid angle, background rate, etc., of separate counters are avoided. This advantage more than compensates for the fact that with the single counter the total counting rate is halved.

The period T_D of the asymmetry cosine curve is found by measuring the time between two peaks, which are separated by about 1600 μsec, and then dividing by the counted number of cycles between the peaks. Details of the method are given in Sec. IV.

The Principal Problems in the Method

The method just described raises experimental problems which can be sorted into three main categories: (1) Determination of the average of the magnetic field the electrons experience while in the trap. In order to hold the electrons, the magnetic field must be slightly nonuniform; therefore, the effective value must be obtained from a three-dimensional map of the field, together with information about the orbits of the electrons. (2) The evaluation of, and reduction of, stray electric fields due to surface charge effects, in the trap. The radial component of an electric field causes shifts in the cyclotron frequency and the spin precession frequency which are not the same; consequently, it affects the difference frequency. (3) Systematic and statistical errors in the measurement of the difference frequency. These include counting statistics, time measurements, etc.

III. APPARATUS

Vacuum Chamber

The main vacuum chamber is 12 in. in diameter and 18 ft long. It is made of six sections, of approximately equal length, bolted end to end by means of flanges. All the inner parts of the apparatus are therefore accessible. The glass insulation for the 100-keV electron gun (see Fig. 1) and an oil diffusion pump are located at the left end of the pipe. The center of the trapping region is about $7\frac{1}{2}$ ft from the left end. A VacIon pump is located at the right end. Because the VacIon pump contains permanent magnets, it is located far away from the trapping region. A baffle plate, having a small hole for the electron beam to pass through separates the trapping region and the VacIon pump from the gun and the oil diffusion pump. This permits a pressure differential to be maintained, making it possible to attain the necessary low pressure (about 10^{-7} mm Hg) in the trapping region. Cold traps are not used, except for a freon-refrigerated baffle in the oil diffusion pump line. The envelope and internal parts in the trapping section were designed in such a way that they could be baked in place, but this was not found to be necessary. Needless to say, magnetic materials were avoided.

Internal Components

Inside the vacuum chamber, in the trapping region, there are just four main components: the electron gun, the scattering foils, the counter, and the cylinders which apply the pulsed electric field for catching the electrons in the trap and ejecting them. The spatial arrangement of these components is shown schematically in Fig. 1. The gun is essentially the same as the one previously described.[2] It is capable of delivering 100-mA peak current for 0.2 μsec at the voltages up to 125 kV.

The scattering foils are of commercially available gold leaf ($\sim$0.2 mg/cm^2). The first (polarizing) foil is mounted in a shield which allows only those scattered electrons to emerge which will begin the helical path with about 1-deg pitch.

The single Geiger counter is mounted in such a position that electrons scattered through an angle of about 110° will enter it. This is approximately the angle for maximum asymmetry. A curved slit system between the foil and the counter passes only electrons which have been scattered through this angle and which have not suffered appreciable energy loss. The slit system reduces background (as measured with the analyzing target removed) to less than 1% of the normal counting rate. The counter has a Mylar window of about 2 mg/cm^2 and is filled with 90% argon and 10% methane to 10 cm Hg pressure. A clearing field is maintained in the counter, and at the time of ejection of the electrons from the trap, the voltage is pulsed into the Geiger

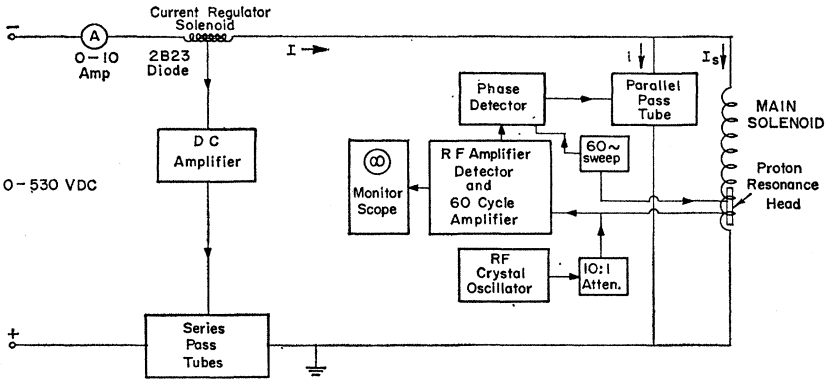

FIG. 2. Block diagram of the magnetic field regulator.

region. The counter counts either one or zero, for each cycle of the system.

The cylinders, by means of which the axial electric trapping and ejecting fields are produced, embody important improvements over those used previously. In the previous apparatus there were two pairs of concentric cylinders, with enough radial separation to accommodate the trapped electrons. This arrangement was optimum for its primary purpose, namely, acceleration of the electrons parallel to the axis. But as we now realize, it was also optimum for the appearance of stray radial electric fields, due to differences in surface conditions or static charges. In the present apparatus there are no inner cylinders; in fact, there is nothing inside the circulating electron cloud. By eliminating all surfaces on which static charges can reside inside the circulating beam, the effect of stray electric fields on the difference frequency is eliminated in first order. Although stray electric fields may still be present, those characterized by lines of force originating and ending on the inner wall of a cylinder have no net effect in first order. Only field lines which originate on the cylinder, go into the region inside the circulating beam, and then out at the end of the trapping region will have a first-order effect. As is shown in the section on results, a significant reduction in electric field effects resulted from this simple structural change in the cylinder system. The cylinders are made of copper and they are baked at about 150°C before being put in place.

Solenoid

Two requirements had to be met in designing the solenoid. (1) The region of magnetic field actually used by trapped electrons is cylindrical in shape, about 6 in. in diameter and 25 in. long. In this region the field must have a high degree of cylindrical symmetry and it must be slightly weaker, by a small fraction of a percent, at the middle than at the ends. (2) Physically the coil assembly was required to be removable from the vacuum chamber assembly to provide accessibility, and it was also required that it be separate from the vacuum chamber to allow for baking the latter. An aluminum spool was made by rolling a plate of $\frac{3}{4}$-in. aluminum into a cylinder 2 ft in diameter and 8 ft long and adding end flanges of 1-in. aluminum. These were helium-welded and machined. This exceedingly rigid spool was wound with eight layers of No. 10 cotton and enamel-insulated wire. Two additional layers were wound on the last 17 in. at each end of the spool. These end-correcting coils were designed by computation on the IBM 704 to give the same field at the ends of the trapping region as at the middle, and it was expected that smaller coils would be used to give the field the very slight bottle shape desired for trapping. As it turned out, the trapping region had the desired field shape without the use of the last-mentioned coils.

To achieve the required physical flexibility, the spool is mounted on a stand, which in turn runs on a short railroad, so that it can be rolled parallel to its axis, toward the VacIon pump, until the section of the chamber containing the trapping region is exposed.

Magnetic Field Regulator

Figure 2 shows a block diagram of the regulator system. A coarse series regulator senses and controls the current labeled I in the figure. A fine parallel regulator senses the magnetic field in the trapping region and controls the small fraction (i) of I which bypasses the solenoid.

The coarse regulator is similar to the one described in the previous report.[2] Its function is only to reduce drift, transients, and ripple to a sufficiently low level for the fine regulator. Drift in the current passed by the coarse regulator is less than 0.05% per day after a 30-min warm-up period.

The sensing element of the fine regulator uses a proton resonance head containing a 12-cc sample of 0.1 molar cupric chloride solution. This is inside an rf coil 4 cm long, which in turn is mounted between two sweep coils 7 cm in diameter. The rf coil constitutes one leg of a tunable resonant circuit having a Q of about 50. A crystal-controlled oscillator drives this resonant circuit through a 10-to-1 attenuator.[6] This method has the

[6] A Pound-Knight oscillator (reference 9) with a crystal in the feedback path (reference 8) was tried. However, the high Q and low frequency of the crystal gave too narrow a circuit bandwidth.

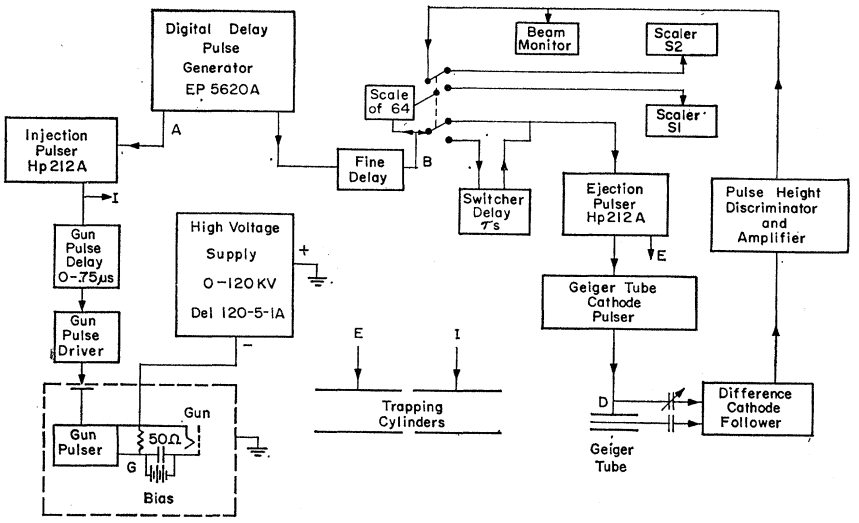

FIG. 3. Block diagram of the timing system.

advantage that the driving source is highly stable while the resonant circuit has a low enough Q to pass the sidebands of the proton-resonance signal. Any one of nine crystals can be selected in a frequency range from 400 to 690 kc/sec, corresponding to magnetic fields at the resonance head in a range from 94 to 162 G.

The remainder of the fine magnetic field regulator is of conventional design.[7] The input to the phase detector is displayed on an oscilloscope as a Lissajous figure, which indicates deviations of the magnetic field from the value determined by the crystal frequency. The signal-to-noise ratio is satisfactorily low. The main sources of noise are microphonics and 60-cps pickup in the resonance head and in the rf amplifier. Fluctuations of such low frequency cannot appear in the magnetic field, however, because of the highly effective "shorted turn" effect of the aluminum spool on which the solenoid is wound. The fine regulator has a time constant of 5 sec, so it does not follow ac pickup, microphonics, or rapid transients. The drift in the magnetic field has been measured and found to be less than one part in 10^5 per day.

Apparatus for Mapping the Magnetic Field

The magnetic field in the trapping region is mapped by means of a proton resonance head similar to the one used for regulation of the field. This mapping head is inserted into the trapping region by removing a section of vacuum chamber between the trapping region and the VacIon pump. In this way, the field can be measured with the trapping cylinders, counting equipment, and vacuum pumps in their normal positions. The mapping head is mounted in such a way that it can be moved in azimuth and parallel to the axis of the pipe but at a fixed radius equal to that of the trapped electron cloud.

[7] M. E. Packard, Rev. Sci. Instr. **19**, 435 (1948).
[8] R. J. Blume, Rev. Sci. Instr. **29**, 574 (1958).

A Pound-Knight[9] marginal oscillator is used to detect resonance. Of several circuits tried, this one seemed to give the best combination of sensitivity and versatility. The oscillator frequency is measured with a Hewlett-Packard 523D frequency counter which is calibrated against WWV.

Timing System

A block diagram of the timing system is shown in Fig. 3. The heart of the system is an Electro-Pulse 5620 A digital delay generator. It provides two pulses whose spacing can be varied from 1 to 10 000 μsec in 1 μsec steps. A crystal oven has been added to the standard clock oscillator to provide additional frequency stability. The clock rate has been measured by comparing it to WWV with a frequency counter.

The timing sequence is as follows. (1) Pulse A triggers the injection pulser which applies negative 70 V to cylinder I. (2) The gun is pulsed giving a helical beam in the trapping region. (3) The voltage is removed from cylinder I, thus trapping electrons. The timing of this event is critical and is controlled by the gun pulse-delay line. (4) After the selected trapping time, pulse B triggers the ejection pulser which applies a negative voltage to cylinder E, ejecting electrons in the direction of the Geiger counter. At the same time a pulse has activated the Geiger counter, so that if an electron is scattered into it, a count is registered. (5) Ejection and Geiger counter voltages are removed and the machine is ready for another cycle. The normal repetition rate is 500 cps.

The scale of 64 circuit shown in Fig. 3 activates an electronic switch every 64 machine cycles. The switch alternately switches the trapping time between t (set by operator) and $t+\frac{1}{2}T_D$ and simultaneously switches the Geiger counter output between scalers $S1$ and $S2$. (See Sec. II for a discussion of this method of measuring

[9] R. V. Pound and W. D. Knight, Rev. Sci. Instr. **21**, 219 (1950).

the asymmetry.) The switcher delay is set to about $\frac{1}{2}T_D$. This setting is not critical; an error of $\pm 50\%$ would reduce the asymmetry amplitude by only 30%.

Except for the timing-pulse generator and the switcher, the timing system is similar to the one which is described in detail in the previous publication.[2] However, many of the "home-brew" circuits have been replaced with commercially made equipment and, as a result, the stability and reliability of the timing system have been improved.

IV. MEASUREMENTS AND ANALYSIS

Mapping of the Magnetic Field

The magnetic field at the beam radius is measured as a function of azimuth and axial distance from the center of the trapping region. The field is found to vary with azimuth, the maximum variation from the average being about 30 parts in 10^6. The average of four azimuthal measurements at each setting of z is used for computing the average field experienced by the circulating electron. In Fig. 4 the azimuthally averaged field, plotted against z, is compared to the field B(Mon) measured by the fixed proton resonance monitor head located in the solenoid. The proton resonance head which measures B(Mon) is similar to the ones used for the regulation and the mapping of the magnetic field. The field at this monitor head is measured periodically during the mapping of the field so it serves as a check on the field regulator.

The field was mapped several times, on different days, and before and after the solenoid had been moved and then replaced. There were no appreciable differences in the results. The data from two such field mappings were averaged to obtain Fig. 4.

Evaluation of the Time-Averaged Magnetic Field and Pitch Correction Term

As noted earlier, although the magnetic field in the laboratory system does not change with time, the magnetic field experienced by the electron in its motion in the "bottle" does vary with time. This time average must be evaluated. To do so it is necessary to analyze the motion of the electron.

The time-averaged magnetic field which an electron sees while trapped between coordinates z_1 and z_2 is

$$\bar{B}_z(z_1)=\frac{2}{T(z_1)}\int_{z_1}^{z_2} B_z\frac{dz}{v_z}, \tag{3}$$

where $T(z_1)$ is the period of the axial oscillation and v_z is the instantaneous axial velocity in the trap. The latter quantity is found from the axial energy relationship

$$\tfrac{1}{2}mv_z^2=\frac{ev_\theta}{c}\int_{z_1}^{z_2} B_r dz, \tag{4}$$

where v_θ is the azimuthal component of the velocity and is nearly constant everywhere in the trap.

Equation (4) can be expressed in terms of B_z. It can be shown[10] that, for the magnetic field in the trapping region, the following relationship is good to 1 part in 20 if $|z_1-z|>5$ cm:

$$\int_{z_1}^{z} B_r dz=\frac{R}{2}[B_z(z_1)-B_z(z)], \tag{5}$$

where R is the beam radius. Equations (4) and (5) are now used to find the instantaneous axial velocity in terms of measured quantities

$$v_z=\{(ev_\theta R/mc)[B_z(z_1)-B_z(z)]\}^{1/2}. \tag{6}$$

The quantity actually measured in the field mapping process is $(B_z^2+B_r^2)^{1/2}$. This differs from B_z by less than 1 part in 10^7 in the trapping region. Therefore, for purposes of Eq. (6) we use the measured values of $(B_z^2+B_r^2)^{1/2}$ as $B_z(z)$. From Eq. (6) we see that the value of z_2, the amplitude of oscillation in the left-hand side of the trap, is found from

$$B_z(z_2)=B_z(z_1), \tag{7}$$

where z_1 is some chosen amplitude in the right-hand side of the trap. Therefore, the trapped electrons oscillate between regions of equal magnetic field intensity.

The period $T(z_1)$ of electrons with amplitude z_1 is given by

$$T(z_1)=2\int_{z_1}^{z_2}\left(\frac{mc}{cv_\theta R}\right)^{1/2}\frac{dz}{[B_z(z_1)-B_z(z)]^{1/2}}. \tag{8}$$

Substitution of Eqs. (6) and (8) into Eq. (3) and simplification of the result gives

$$\bar{B}_z(z_1)=B_z(z_1)-\int_{z_1}^{z_2}[B_z(z_1)-B_z(z)]^{1/2}dz\Big/\int_{z_1}^{z_2}\frac{dz}{[B_z(z_1)-B_z(z)]^{1/2}}. \tag{9}$$

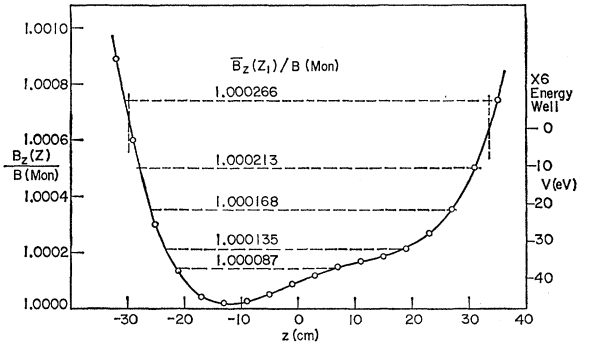

FIG. 4. The magnetic field in the trapping region, averaged in azimuth, relative to the magnetic field at the monitor head. The values given for $\bar{B}_Z(Z_1)$ are those corresponding to electrons in the energy well at the levels indicated by the dashed lines.

[10] D. T. Wilkinson, Ph.D. thesis, University of Michigan, 1962 (unpublished).

Therefore, the time-averaged magnetic field experienced by electrons with amplitude z_1 can be found from Eq. (9) by integrating functions of the measured magnetic field. These integrals have been performed graphically for the magnetic field shown in Fig. 4. Five values for z_1 were chosen: 35, 31, 27, 19, and 7 cm. The results for $\bar{B}_z(z_1)$ are given in Fig. 4 on the horizontal dashed lines which terminate at the corresponding values of z_1 and z_2.

The maximum amplitude in the trap is indicated in Fig. 4 by a vertical dashed line at 33.7 cm. This is the position of the end of the trapping cylinder and the leading edge of the analyzing target. The maximum excursion in the left side of the well is then found to be -30 cm. Therefore, we see from Fig. 4 that the time-averaged magnetic field, experienced by electrons with any possible amplitude in the trap must be in the following range:

$$1.000\,05 < \bar{B}_z/B(\text{Mon}) < 1.000\,24. \tag{10}$$

This range can be narrowed by making use of certain experimental results. For low ejection pulse voltages, only electrons trapped with large amplitudes are spilled out of the energy well. We have found that as the ejection voltage is increased from zero, counts begin to appear at about 1 V. This means that there are electrons trapped with nearly the maximum amplitude. As the ejection voltage is increased further, a saturation counting rate is reached. The ejection voltage corresponding to this saturation rate is a measure of the lowest energy level to which the well is populated. Therefore, if we find the amplitude corresponding to this lowest energy level a new lower limit can be set in (10).

The energy level of an electron trapped with amplitude z_1 is given by

$$V(z_1) = -\frac{ev_\theta}{c}\int_{33.7}^{z_1} B_r dz, \tag{11}$$

where the maximum amplitude has been assigned the energy level zero. Equation (5) is then used to get

$$V(z_1) = -\tfrac{1}{2}(ev_\theta R/c)[B_z(33.7) - B_z(z_1)]. \tag{12}$$

Therefore, the energy well has the same shape as the magnetic field map. For example, the energy scale on the right-hand side of Fig. 4 corresponds to 81-kV electrons in a magnetic field of about 129 G. Using Eq. (12) the energy scale can be found for any setting of the magnetic field and electron energy.

The final data of this experiment were taken at four different settings of field and energy. Each setting is denoted by the number of the crystal to which the magnetic field is locked ($X3$, $X6$, $X8$, or $X9$). The values of several experimental parameters are given in Table I for each of these four settings. The ejection voltages listed in Table I correspond to the saturation counting rates and are the values used for the final asymmetry runs. It should be noted that the ejection voltage used at each setting was less than the maximum well depth.

TABLE I. Some experimental parameters for each final data setting. The minimum well amplitude is the smallest amplitude from which electrons are ejected from the well.

Setting		$X3$	$X6$	$X8$	$X9$
Crystal frequency	(kc/sec)	650.12	550.01	450.12	400.08
Magnetic field	(G)	153	129	106	94
Electron energy	(keV)	114	81	56	45
Maximum well depth	(eV)	−65	−47	−32	−27
Ejection voltage	(V)	18	26	23	15
Minimum well amplitude	(cm)	30.4	25.0	18.5	25.0

The minimum amplitude which electrons can have and still reach the target on ejection is found from graphs like Fig. 4. For example, the $X6$ ejection voltage is 26 V and we see from Fig. 4 that this corresponds to an amplitude of 25 cm. No electrons with smaller amplitudes can be ejected. The minimum well amplitude is listed in Table I for each of the four final settings. Using these minimum amplitudes, we may now go back and assign new lower limits in (10). The resulting time-averaged magnetic fields for trapped electrons become, then,

$$\begin{aligned}\bar{B}_z/B(\text{Mon}) &= 1.000\,220 \pm 0.000\,020 \text{ for } X3,\\ &= 1.000\,198 \pm 0.000\,042 \text{ for } X6,\\ &= 1.000\,188 \pm 0.000\,052 \text{ for } X8,\\ &= 1.000\,198 \pm 0.000\,042 \text{ for } X9,\end{aligned} \tag{13}$$

where the uncertainties include all possible well levels from which electrons are ejected.

The time-averaged value of the pitch correction term in Eq. (2) can also be calculated from the magnetic field map. We wish to evaluate the time-averaged square of the axial velocity in the trap. From Eqs. (6) and (8)

$$\langle v_z^2\rangle_{\text{av}} = \frac{ev_\theta R}{mc}\int_{z_1}^{z_2}[B_z(z_1) - B_z(z)]^{1/2}dz \Big/ \int_{z_1}^{z_2}\frac{dz}{[B_z(z_1) - B_z(z)]^{1/2}}. \tag{14}$$

Notice that these integrals have already been evaluated in connection with Eq. (9). The values found for the pitch correction term for the four final settings are

$$\begin{aligned}\frac{\gamma a}{\gamma+1}\frac{\langle v_z^2\rangle_{\text{av}}}{c^2} &= (8.7 \pm 1.4)\times 10^{-8} \text{ for } X3,\\ &= (5.0 \pm 2.2)\times 10^{-8} \text{ for } X6,\\ &= (3.0 \pm 2.0)\times 10^{-8} \text{ for } X8,\\ &= (2.8 \pm 1.2)\times 10^{-8} \text{ for } X9,\end{aligned} \tag{15}$$

where 0.001 16 was used for a and the uncertainties quoted are due to possible errors in choosing the values of z_1 for Eq. (14). Therefore, these uncertainties come from the same source as the uncertainties in

$\bar{B}_z/B$(Mon). The values given in Eqs. (13) and (15) are used in Part IV to find the experimental result for a.

Measurement of the Difference Frequency

The ratio of the counting rates at the trapping times t and $t+\frac{1}{2}T_D$ (see Sec. II) is measured and plotted as a function of trapping time t. This is referred to as the asymmetry curve. The period T_D of the resulting cosine curve is found by finding the time between two widely separated maxima and then dividing by the counted number of cycles between these maxima. Thus, the problem is twofold: The accurate measurement of trapping times corresponding to two maxima, and the determination of the number of cycles between the maxima chosen.

Data which would lead to the precise determination of maxima in the asymmetry curve were taken in two regions of trapping time: approximately 300 and 1900 μsec. At trapping times of 300 μsec and longer the electron cloud retains none of the structure associated with the injection, so the number of electrons released from the trap is a smooth and slowly decreasing function of the trapping time. 1900 μsec is the longest trapping time at which reasonable counting rates are obtained.

In all, 36 separate pairs of runs were made for the determination of T_D (9 runs at each of the four magnetic field settings in Table I). A run consisted of measuring about 2 cycles of the asymmetry curve. Runs were always taken in pairs, one in the region of 300 μsec and one in the region of 1900 μsec. The data for the first four pairs of runs (one pair at each magnetic field setting) are shown in Fig. 5. In connection with these four pairs of runs, enough data were also taken at intermediate trapping times to make possible the determination of the number of cycles N between the two end points. A similar determination of N was not necessary for the next 32 pairs of runs because the variation in the time difference between the two end points, from one pair of runs to another, was much less than a full period. In other words, once N had been established in the first four pairs of runs, there was no possibility of being in error by a whole cycle in the subsequent measurements.

The procedure for measuring N is as follows: (1) An estimate is made of the location (on the time axis) of the two end maxima, M_{300} and M_{1900}. (2) The position of another maximum, at about 350 μsec, is located by measuring and plotting a 2-cycle interval as in the other cases. Enough data are taken all the way along the time axis between 300 and 350 μsec so that the number of cycles can be counted. This makes possible the determination of T_D for the 300–350 μsec interval, to about $\pm\frac{1}{2}\%$. From this, N for the 300–1900 μsec interval can be estimated to the same relative accuracy, which amounts to at most ± 4 cycles. (3) Enough data are taken midway between M_{300} and M_{1900} to find whether a maximum or minimum occurs at that place. Thus it is determined whether N is even or odd. (4)

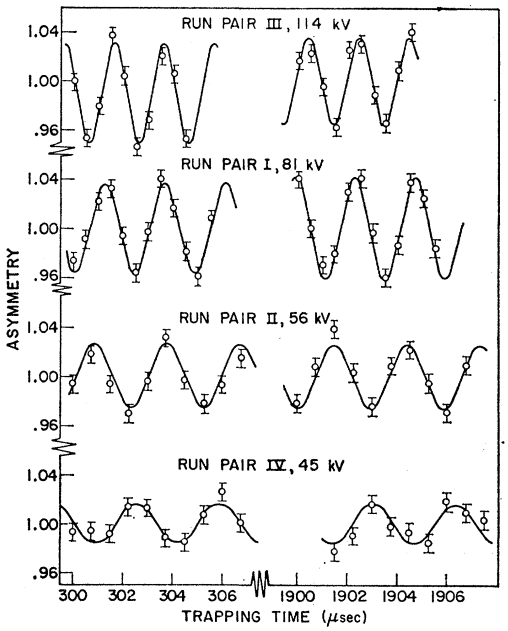

FIG. 5. Four pairs of asymmetry runs, each pair consisting of approximately two cycles in the neighborhood of 300- and of 1900-μsec trapping time. The asymmetry is the ratio of the counting rates at t and $t+T_D/2$ as explained in Sec. IV.

Enough data are taken about $\frac{1}{3}$ of the way between M_{300} and M_{1900} to establish which of $N-1$, N, or $N+1$ is divisible by 3. Only a single value of N can satisfy the results of all of the steps described.

The resonant frequency of the monitor head f(Mon) was also measured periodically during each run. This served as a check on the magnetic field regulator and also gave a means of connecting the measurements of $\bar{B}_z$ and T_D which are, of necessity, made at different times.

Evaluation of the Difference Frequency

An IBM 709 computer was used to obtain the least-squares fit of a curve of the form $y=A\cos(\omega t+\phi)+C$ to each of the runs, a run being a sequence of points extending over approximately two cycles. Using the value of ϕ, given by the least-squares fit, the value of the trapping time corresponding to a maximum in the asymmetry curve was found, for each run. Table II gives all of these values. The values for the runs in the region of 300 μsec are labeled M_{300} and those for the runs in the region of 1900 μsec are labeled M_{1900}. Inasmuch as each run included at least two cycles, an arbitrary selection had to be made. In the 300-μsec runs the maximum at the shortest trapping time was selected for listing in the table, and for the 1900-μsec runs the one at the longest trapping time was selected.

The difference between the times corresponding to M_{300} and M_{1900} divided by N gives T_D in μsec. The 36 values of this quantity are given in Table II. Since the magnetic field regulator was reset after each pair of

TABLE II. The results of the 36 pairs of asymmetry runs. The results of run XXIII were not included in the final calculation, for reasons stated elsewhere.

Run pair	Setting	M_{1900}	M_{300}	N	T_D (μsec)	T_D f(Mon)
III	$X3$	1902.375	301.600	793	2.01863	1.311379
VII	$X3$	1902.150	301.350	793	2.01866	1.311394
XI	$X3$	1904.475	301.650	794	2.01867	1.311421
XV	$X3$	1904.250	301.400	794	2.01870	1.311432
XVIII	$X3$	1902.700	301.900	793	2.01866	1.311428
XXII	$X3$	1900.700	301.925	792	2.01866	1.311412
XXVI	$X3$	1902.550	301.800	793	2.01860	1.311375
XXIX	$X3$	1902.675	301.850	793	2.01869	1.311432
XXXV	$X3$	1904.850	302.075	794	2.01861	1.311364
I	$X6$	1904.700	301.275	672	2.38605	1.311366
V	$X6$	1904.825	301.425	672	2.38601	1.311358
IX	$X6$	1902.450	301.450	671	2.38599	1.311323
XIII	$X6$	1902.650	301.600	671	2.38607	1.311406
XVII	$X6$	1902.725	301.750	671	2.38595	1.311325
XXI	$X6$	1902.675	301.600	671	2.38610	1.311410
XXV	$X6$	1902.450	301.400	671	2.38607	1.311408
XXX	$X6$	1902.575	301.550	671	2.38603	1.311372
XXXIII	$X6$	1902.850	301.825	671	2.38603	1.311376
II	$X8$	1904.400	300.850	550	2.91554	1.311363
VI	$X8$	1904.475	300.900	550	2.91559	1.311359
X	$X8$	1904.525	301.050	550	2.91541	1.311261
XIV	$X8$	1904.800	301.275	550	2.91550	1.311334
XIX	$X8$	1904.600	301.125	550	2.91541	1.311243
XXIII	$X8$	1907.425	301.200	551	2.91511	1.311123
XXVII	$X8$	1904.750	301.275	550	2.91541	1.311313
XXXII	$X8$	1904.825	301.375	550	2.91536	1.311256
XXXVI	$X8$	1905.100	301.625	550	2.91541	1.311276
IV	$X9$	1906.425	302.575	489	3.27986	1.311222
VIII	$X9$	1906.525	302.575	489	3.28006	1.311279
XII	$X9$	1906.450	302.700	489	3.27965	1.311129
XVI	$X9$	1906.775	302.925	489	3.27986	1.311180
XX	$X9$	1903.550	302.900	488	3.28002	1.311254
XXIV	$X9$	1903.400	302.800	488	3.27992	1.311246
XXVIII	$X9$	1906.850	312.625	486	3.28030	1.311372
XXXI	$X9$	1906.800	302.925	489	3.27991	1.311226
XXXIV	$X9$	1910.425	309.650	488	3.28028	1.311348

runs, the value of f(Mon) varied slightly between pairs of runs taken at the same setting of magnetic field. Therefore, the quantity which is averaged over the 9 pairs of runs at each setting is $T_D f$(Mon). The 36 values of $T_D f$(Mon) are given in Table II.

During the averaging process, one pair of runs (XXIII) was found to give a result which was far out of line with the results of the other 8 pairs of runs in its group. $T_D f$(Mon) for run pair XXIII differed from the average value by more than four times the rms deviation of the other 8 values of $T_D f$(Mon) from their mean, indicating that something was wrong with this measurement. This pair of runs was discarded.

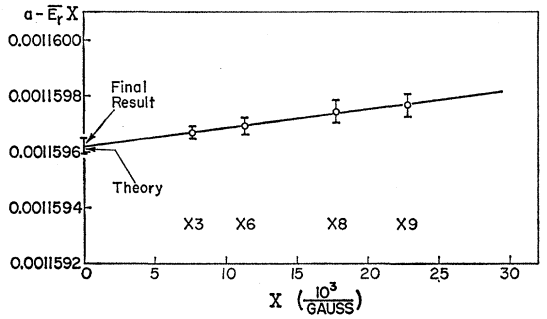

FIG. 6. The measured results plotted against X where $X=1/\gamma^2\beta^2\bar{B}_z$.

The average value of $T_D f$(Mon) for the four settings of magnetic field (and electron energy) obtained from the four groups of 9 (8 in one case) pairs of asymmetry runs are:

$$\begin{aligned} T_D f(\text{Mon}) &= 1.311\,382 \pm 0.000\,013 \text{ for } X3, \\ &= 1.311\,348 \pm 0.000\,016 \text{ for } X6, \\ &= 1.313\,279 \pm 0.000\,020 \text{ for } X8, \\ &= 1.313\,227 \pm 0.000\,026 \text{ for } X9. \end{aligned} \tag{16}$$

The error given in each case is the result of combining two errors by taking the square root of the sum of their squares. One of the errors is an estimate of the error in measuring f(Mon). The other error is the standard error of the mean obtained from the averaging of the results of the 9 (8 in one case) pairs of runs.

An adjustment of 18 parts in 10^6 is included in the values given in Eq. (16) to bring the frequency scale of the trapping time oscillator into agreement with the standard frequency of WWV. This adjustment is not included in the figures of Table II.

V. COMPUTATION OF THE g FACTOR

The results of the previous section are now used to evaluate the left-hand side of Eq. (2). This quantity can be written as follows:

$$\frac{\omega_D}{\bar{\omega}_0} = \frac{mc}{e}\gamma_p \frac{B(\text{Mon})}{\bar{B}_z} \frac{1}{T_D f(\text{Mon})}, \tag{17}$$

where γ_p is the gyromagnetic ratio for protons in water. The last two factors on the right-hand side of Eq. (17) were evaluated in the previous section. The value of the particular combination of constants $mc\gamma_P/e$ has been measured very accurately by Franken and Liebes.[11] Their value, corrected to apply to protons in water, is $1/(657.465\pm0.006)$. Substituting this result and the values from Eqs. (13) and (16) into Eq. (17) we obtain the measured values of $\omega_D/\bar{\omega}_0$ at each of the four settings given in Table I. The values in Eq. (15) for the pitch correction terms are then added in and the following results are obtained for the three remaining terms in Eq. (2):

$$\begin{aligned} a - \frac{1}{\beta\gamma^2}\frac{\bar{E}r}{\bar{B}_z} + \frac{f^2\beta^2}{8a} &= 0.001\,159\,672 \pm 0.000\,000\,018 \text{ for } X3, \\ &= 0.001\,159\,690 \pm 0.000\,000\,031 \text{ for } X6, \\ &= 0.001\,159\,743 \pm 0.000\,000\,045 \text{ for } X8, \\ &= 0.001\,159\,775 \pm 0.000\,000\,045 \text{ for } X9. \end{aligned} \tag{18}$$

[11] P. Franken and S. Liebes, Phys. Rev. **104**, 1197 (1956).

The uncertainty quoted for each setting is the square root of the sum of the squares of the independent experimental errors. The sources and magnitudes of these experimental errors are discussed in detail in Sec. VI.

The magnitudes of the two correction terms in Eq. (18) are estimated from the energy dependence of the measured results. In Fig. 6 the values on the right-hand side of Eq. (18) are plotted against X, where X is $1/(\beta\gamma^2\bar{B}_z)$ and is the multiplier of $\bar{E}_r$. The linearity of the results, when plotted against this quantity, leads us to make the following assumptions: (1) The observed energy dependence of the results of Eq. (18) is due to a constant radial electric field in the trapping region. (2) The electron has no EDM ($f=0$).

The two assumptions are justified by the fact that, in the plot used, an electric field would be expected to produce a straight line relationship with a slope, while an EDM would be expected to introduce curvature. Later the second assumption is relaxed and the effect of a possible EDM is calculated.

On the basis of the two assumptions above, a straight line is fitted to the points in Fig. 6. The intercept of this line with the ordinate ($X=0$) gives the measured value of the g factor anomaly:

$$a=0.001\,159\,622\pm0.000\,000\,027. \tag{19}$$

The uncertainty quoted is the estimated error in locating the intercept and is discussed in Sec. VI. The slope of the fitted line gives the value for the average radial electric field as

$$\bar{E}_r=(-1.9\pm1.2)\times10^{-3}\ \text{V/cm}. \tag{20}$$

If we now relax the second assumption above and allow the possibility of a nonzero EDM, then another least-squares fit can be performed and the three parameters a, $\bar{E}_r$, and f can be determined. The values obtained are

$$a=0.001\,159\,609, \tag{21a}$$

$$\bar{E}_r=2.0\times10^{-3}\ \text{V/cm}, \tag{21b}$$

$$f=3.7\times10^{-5}\ (\text{EDM}=4\times10^{-16}\ \text{cm}\times e). \tag{21c}$$

Therefore, even upon the assumption that there is a finite EDM, our data give a value for a which is within the uncertainty limits in Eq. (19). For this reason, and because there is as yet no separate evidence that f is not zero, we quote the value in Eq. (19) as our final result.

There is some experimental evidence to support the first of the two assumptions above. For the early stages of the present experiment, trapping cylinders were used inside the beam radius. As pointed out in Sec. II, this trapping geometry greatly enhances radial electric fields due to surface charges. Some of these results (Early g factor III) are shown in Fig. 7. This figure is similar to Fig. 6 except that the vertical scale has been contracted by a factor of 10. Notice the steep slope of the early results. The slope was decreased by a factor of 3 when the trapping cylinders were polished, and it was almost eliminated by removing the inner cylinders. These results indicate that electric fields due to surface charging are present in the trapping region and that they are not strongly dependent upon the energy and magnetic field settings. For comparison purposes, the results of the previous experiment (g factor II) are also shown in Fig. 7.

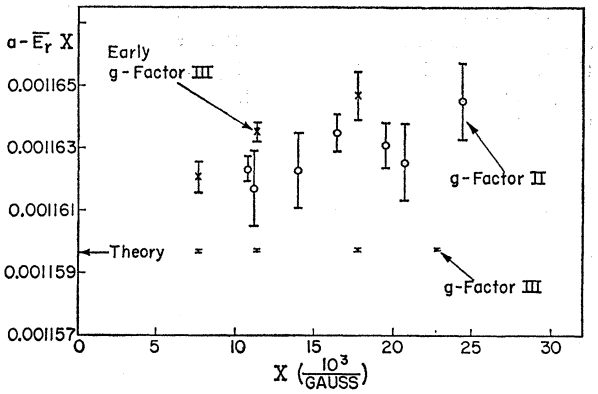

FIG. 7. Comparison of the g-factor II results (Schupp, Pidd and Crane) with the present (g factor III) results. The results labeled early g factor III are those obtained using trapping cylinders similar to those used in II. The lower line of points (g factor III) shows the final results, obtained with the improved trapping cylinder system.

VI. ERRORS

Three types of error contribute to the error in the final result as given in Eq. (19). First, there are the errors of measurement, which are of both instrumental and statistical origin. Second, there is an error associated with the fitting of the straight line to the data points, in Fig. 6, and the extrapolation by which the final value for the g factor is found. Finally, there is the error (difficult to estimate) associated with the decision to use a straight line for fitting the points and making the extrapolation, i.e., the question as to the validity of the two assumptions preceeding Eq. (19).

TABLE III. Possible experimental errors. The sources of error in each category are given in the text.

Category	$X3$ (ppm)	$X6$ (ppm)	$X8$ (ppm)	$X9$ (ppm)
A	±20	±42	±52	±42
B	∓12	∓19	∓17	∓10
C	± 6	± 8	±11	±16
D	± 8	± 9	±11	±13
E	± 9	± 9	± 9	± 9
Limit of error	±31	±49	±66	±70
Estimate of error	±16	±27	±39	±39

The errors of measurement are grouped into five categories, depending upon how they enter the calculation of the final result. Table III gives the error which each category introduces into the values on the right-hand side of Eq. (18). The sources of error which contribute to each category are listed and explained below.

A. The error in the determination of the average magnetic field experienced by electrons in the trap. This error arises mostly from errors in assigning an average amplitude (z_1) to the axial oscillations of the trapped electrons. Other errors, which have been included under this category, are (1) estimated errors in the mapping of the magnetic field and (2) errors from the use of Eq. (5) in the calculation of the average magnetic fields. The errors from this category are included in Eq. (13).

B. The error in the value of the pitch correction term given by Eq. (15). Most of this error arises from errors in assigning an average amplitude (z_1) to the axial oscillations of the trapped electrons. However, here the effect on the final result is opposite to that of the error of category A. Therefore, the signs of the category B errors are reversed.

C. The error in the measurement of T_D. The standard error in the mean of the results of each group of 9 pairs of runs is given in Table III. This error includes: (1) statistical error from the counting process and from the fitting of cosine curves to the data, (2) errors in resetting the magnetic field, electron energy, and other experimental parameters, and (3) error due to slow changes in surface conditions of the trapping cylinders.

D. The error in f(Mon). A value for the resonant frequency of the monitor proton resonance head was assigned to each of the 36 final runs. The error in this value includes (1) error in locating the true resonance, and (2) error due to small drifts in the value of f(Mon) during the course of a run. The errors from categories C and D are both included in Eq. (16).

E. The error in the value of the quantity $mc\gamma_p/e$ (see Sec. V).

Attention is called to the fact that several sources of systematic error have been eliminated in the present experiment by measuring T_D between two maxima in the asymmetry curve, rather than between zero trapping time and one maximum. These are (a) a "zero correction" to the trapping time, which would involve the delays in the pulse circuits and the time spread of the beam, (b) the effect of the electric trapping pulse on the polarization during the first and final passes of the bunch across the center of the trap, and (c) the effect of odd-power terms in the equation for the pitch correction. The latter follows from the fact that the number of passes through the trap, in the measured interval in the asymmetry curve, is necessarily even.

It should be pointed out that the errors in categories A, B, D, and E are limits of error. For example, the error quoted in Category A gives a range of values for $\bar{B}_z/B$(Mon) which includes the values corresponding to all levels of the energy well from which electrons are ejected. On the other hand, the error in category C is of statistical origin and the value given is the standard error of the mean. We believe that the relatively large quantity of data used in the measurement of T_D justifies the use of a statistical error in this case.

Our estimate of the experimental error is obtained by taking the square root of the sum of the squares of the independent experimental errors. Since errors A and B have the same source (uncertainties in the average amplitude in the well), they are added together before being combined with errors C, D, and E. Thus, the "estimate of error" is given by $[(A+B)^2+C^2+D^2+E^2]^{1/2}$. Errors A and B have opposite signs and, therefore, tend to cancel. This cancellation is quite good for our $X3$ setting. The values of the estimate of error, for the four magnetic field settings, are given in Table III and in Eq. (18).

The error of the final result quoted in Eq. (19) includes the error in locating the intercept of the straight line in Fig. 6. There are several ways in which this error can be evaluated. We have chosen the following method because, in view of the types of errors involved, it seems to be the most reasonable. The $X3$ measurement is the most accurate and the most heavily weighted in fitting the straight line to the measured results. Therefore, we have assigned an error to the final result which includes the intercepts of lines fitted to the measured points $X9$, $X8$, and $X6$, and to any point on the $X3$ error flag (see Fig. 6). This procedure gives a relatively conservative estimate of the final error.

If the two assumptions preceding Eq. (19) were not valid, a further error would be introduced in the final result. The error which would result from relaxing only the second assumption has been shown to be small (see discussion of Eqs. 21). However, if both assumptions were invalid, then the straight-line fit used to obtain the final result would be invalid. That is, if $\bar{E}_r$ were not constant, then the linearity of the four points in Fig. 6 would have to be ascribed to an accidental masking of the effect of an EDM by changes in $\bar{E}_r$. In view of the rather wide range of energy used (45 to 114 kV) and the excellent linearity of the four measured points, this possibility seems to us to be quite remote, and it is ignored in arriving at the final result.

VII. CONCLUDING REMARKS

The experimental results for a are now compared to the current theoretical value. The first two terms[12–14]

[12] J. Schwinger, Phys. Rev. **73**, 416 (1948); **74**, 1439 (1948); **75**, 651 (1949); **76**, 790 (1949).
[13] C. M. Sommerfield, Phys. Rev. **107**, 328 (1957); Ann. Phys. (N. Y.) **5**, 26 (1958).
[14] A. Petermann, Helv. Phys. Acta **30**, 407 (1957).

in the theoretical expression give

$$a(\text{theory})=\alpha/2\pi-0.328\alpha^2/\pi^2=0.001\,159\,615 \quad (22)$$

for $\alpha^{-1}=137.0391$.[15] The experimental value is given in Eq. (19) and may be written in the following way:

$$a(\text{exp})=\alpha/2\pi-(0.327\pm0.005)\alpha^2/\pi^2. \quad (23)$$

Therefore, the theoretical and the experimental coefficients in the α^2 term are in agreement within about 1%. The two expressions for a above are set forth without the inclusion of an uncertainty figure for α. For the purpose of displaying the agreement between the theoretical and experimental values of a, this simplified treatment seems to be justified by a comfortable, but not excessively wide, margin. The uncertainty in α^{-1}, as estimated by Dumond and Cohen[15] is ±0.0006. When this is inserted into (22), it propagates into an uncertainty of ±5 parts in 10^6 in a(theory). This uncertainty is smaller, by a factor of about five, than the present experimental uncertainty in a.

Some remarks may be in order here as to the possibility of, and the usefulness of, further improvements in the precision of the experiment. As to the possibility: We estimate that with an intensive effort (at least another year's work) the precision might be improved by a factor 2 or 3. However, we can think of no essential change that could be made in the method, which would lead to a substantial jump in precision, such as was obtained between the previous experiment and the present one.

As to the usefulness of more experimental precision: Superficially it might appear that we are nearly within reach of being able to give an experimental value for the coefficient of the next higher term in the series, namely the α^3/π^3 term. Although the coefficient of α^3/π^3 has not been computed theoretically, we note that α^3/π^3 itself is 1.2×10^{-8}, and that if the coefficient were one, the effect of the term on a would be about one half the amount of the present experimental uncertainty. The use of improved experimental data for this purpose would be precluded, however, because of the uncertainties in several of the other physical constants that would be involved. The fact that the problem would become complicated in several ways at about the same point in precision is best shown by the following tabulation.

Experimental uncertainty in a	23 parts in 10^6
Uncertainty in a from the uncertainty in $mc\gamma_p/e$	9 parts in 10^6
Uncertainty in a from the uncertainty in α	5 parts in 10^6
Change in a by the addition of α^3/π^3 to (22)	11 parts in 10^6

Thus, while a modest improvement in the precision of the experiment might be of interest in respect to the interrelations among certain of the constants, it would not, at the present time, provide a test of the theoretical formula for a in the order α^3/π^3. Partly for this reason, but mainly for experimental reasons, we here conclude the 10-year effort of the laboratory on the g factor of the free negative electron.

Brief mention may be made of two other possible interpretations of the experimental results. If, arbitrarily, the theoretical result for the g factor is taken to be exactly correct, then deviations of the experimental data from it can be regarded as indications of properties of the electron not included in the theoretical treatment. One of these is an electric dipole moment. This was considered in respect to the earlier g-factor data.[16] Using the present data, a least-squares fit of the left-hand side of Eq. (18) to the values on the right gives $f=3.7\times10^{-5}$. Interpreting this value as an upper limit, we obtain

$$\text{EDM(electron)}<e(4\times10^{-16}\text{ cm}). \quad (24)$$

It has been pointed out to us by Hammer,[17] and also by Petermann,[17] that yet another approach would be to interpret the deviations in terms of the finite size of the electron. These, and perhaps other interesting by-products, might serve as incentives for seeking ways of improving the precision of the measurement.

ACKNOWLEDGMENTS

We wish to thank Professor G. W. Ford and Professor R. R. Lewis for several stimulating discussions of the theory of this experiment. Also we would like to acknowledge the remarkable skills of Harry Westrick,[18] who constructed the apparatus. Significant contributions were also made by Marshall Berman, Andrew Sabersky, Neil Savage, and Charles Alexander.

[15] J. W. M. DuMond and E. R. Cohen, Phys. Rev. Letters **1**, 291 (1958).

[16] D. F. Nelson, A. A. Schupp, R. W. Pidd, and H. R. Crane, Phys. Rev. Letters **2**, 492 (1959).

[17] C. L. Hammer and A. Petermann (private communications).

[18] Now deceased.